The fiber break evolution process in a 2-D epoxy/glass multi-fiber array

The Fiber Break Evolution Process in a 2-D Epoxy/Glass Multi-Fiber Array

E.D. McCarthy, J.H. Kim, N.A. Heckert, S.D. Leigh, J.W. Gilman, G.A. Holmes

PII: S0266-3538(14)00375-3
DOI: http://dx.doi.org/10.1016/j.compscitech.2014.10.013
Reference: CSTE 5962

To appear in: *Composites Science and Technology*

Received Date: 25 April 2014
Revised Date: 14 September 2014
Accepted Date: 14 October 2014

Please cite this article as: McCarthy, E.D., Kim, J.H., Heckert, N.A., Leigh, S.D., Gilman, J.W., Holmes, G.A., The Fiber Break Evolution Process in a 2-D Epoxy/Glass Multi-Fiber Array, *Composites Science and Technology* (2014), doi: http://dx.doi.org/10.1016/j.compscitech.2014.10.013

The Fiber Break Evolution Process in a 2-D Epoxy/Glass Multi-Fiber Array

E.D. McCarthy[1,3], J.H. Kim[1], N.A. Heckert[2], S.D. Leigh[1], J.W. Gilman[1], G.A. Holmes[1]*

[1] Materials Science and Engineering Division, [2] Statistical Engineering Division

National Institute of Standards and Technology, Gaithersburg, MD, 20899-8541

[3]Current Address: University of Manchester Aerospace Research Institute, Manchester, UK, M13 9PL

* Corresponding author (gale.holmes@nist.gov)

Keywords *composites, interface, interfacial shear strength, E-glass, epoxy resins*

The Fiber Break Evolution Process in a 2-D Epoxy/Glass Multi-Fiber Array

ABSTRACT.

The mechanical integrity of a structural composite is strongly affected by the strength and toughness of the fiber-matrix interface/interphase [1], with interfacial shear strength (IFSS) being generally accepted as the best quantifying metric. The value of the IFSS is not directly measurable, but it can be approximated by several micromechanics based test methods with the value obtained being dependent on the choice of the model. The most popular of these test methods is the embedded single fiber fragmentation test (SFFT) which provides the experimental data needed to estimate the IFSS: (a) mean fragment length at saturation and (b) fiber strength at the critical fragment length.

Because the IFSS is used in unidirectional composite models to predict strength and failure behavior, where the interaction between fibers can be important, the validity of extrapolating from test results based upon the repeated failure of a single isolated fiber has often been questioned. In this paper, the spatial distribution of fiber breaks in a 2-D array of glass fibers is compared with break locations observed from SFFT specimens. In both cases, the break locations in each fiber were found to evolve to a uniform distribution, thereby confirming that the ordered fragment lengths from the repeated fracture process conforms for both SFFT and multi-fiber fragmentation test (MFFT) specimens to a cumulative distribution function (CDF) derived by Whitworth [2-5]. The array break density was also observed to be less than the break density in isolated fibers, and break locations across array fibers were observed to be highly coordinated and mostly aligned.

KEYWORDS: composites, interface, interfacial shear strength, E-glass, epoxy resins.

The Fiber Break Evolution Process in a 2-D Epoxy/Glass Multi-Fiber Array

INTRODUCTION

The mechanical integrity of a structural composite is strongly affected by the strength and toughness of the interface/interphase that is formed between the continuous matrix phase, or resin, and the reinforcing phase, normally consisting of closely spaced carbon or glass fibers [1]. Interfacial shear strength (IFSS) is the generally accepted parameter for quantifying the strength of the matrix-fiber interface/interphase and is used to model a composite's strength and failure behavior. However, the value of the IFSS is not directly accessible by measurement and must be approximated indirectly from experimental data obtained from micromechanics test methods and a single fiber composite (SFC) model that has been modified for composite analyses.

One mechanical test that generates such data is the single fiber fragmentation test (SFFT) [6-11] which involves the repeated fracture of the embedded fiber to a point called saturation (cessation of fiber breaks). By recording the overall strain and load on the fiber at saturation, as well as the number of breaks (current practice) and associated fragment lengths, an approximate calculation for the IFSS is obtained using models derived from the 'fiber' free body diagram shown in Figure 1. The limitations of the various micromechanical models developed to calculate the IFSS have been well documented [12-22]. The equation for calculating the IFSS, τ_i, has the following general form:

Equation 1

$$\tau_i = r_f f\{l_c\}\sigma_f(l_c)$$

where

r_f is the radius of the fiber

$\sigma_f(l_c)$ is the strength of the fiber at the critical transfer length, l_c [17,23].

$f\{l_c\}$ is a function of l_c with the explicit expression depending on model assumptions with the two most popular models being the Kelly-Tyson (K-T, Equation 1a) and the Cox (Equation 1b) models [24].

The Fiber Break Evolution Process in a 2-D Epoxy/Glass Multi-Fiber Array

Kelly-Tyson Model: $f\{l_c\} = \frac{1}{l_c} = \frac{K'}{\bar{l}_f}$ yields Equation 1a

Cox Model: $f\{l_c\} = \frac{\beta}{2}\frac{sinh(\beta l_c/2)}{cosh(\beta l_c/2)-1}$ yields Equation 1b

$$\beta = \frac{1}{r_f}\left[\frac{E_m}{(1+\nu_m)(E_f-E_m)ln(r_m/r_f)}\right]^{\frac{1}{2}}$$

K'	variability correction factor has a value of 0.75 or 0.668 [25]
E_m, E_f	are the modulus of the matrix and fiber, respectively.
r_m, r_f	are the radius of the matrix and fiber, respectively.
ν_m	is the Poisson's ratio of the matrix.

In reviewing the fragmentation test protocol, Curtin [26] indicated the need to record break locations along the fiber axis within the gauge length of interest, thereby allowing the actual fragment length distribution to be recorded and modeled. Drzal et al. [11] followed this approach and generated a fragment length distribution for two different fibers (sized and unsized) in an epoxy/carbon fiber system. They reported good fits of their fragment length data to a Weibull distribution. However, the Weibull distribution function has not always been successful in modeling fragment length data. Bascom et al. [27] reported that their fragment length data collected from ten separate carbon fibers in epoxy matrices, were not well modeled by a Weibull distribution, which suggested that an alternative statistical approach might be more accurate in representing such data. Others [17,28] have advocated the use of a log normal distribution. In 2009, a possible alternative to using Weibull statistics for fragment length data was proposed by Kim et al. [9], who demonstrated that a uniform distribution could be very successfully applied to describe the spatial arrangement of break centroids along a fiber axis. The application of Uniform Spacings theory gives an explicit equation for the ordered fragment *length* distribution due to Whitworth [2-4].

In 1995, a multi-fiber fragmentation study using 2-D Nicalon fiber arrays showed that the mean fragment length in an array is typically larger than the mean fragment length obtained from the repeated fragmentation of a single fiber [29]. The fragment length was shown to increase with smaller inter-fiber

separation and/or more embedded fibers. Li et al. [29] observed that the Cox-type shear-lag theories, which are the basis for composite models, predict the opposite effect. These results led the researchers to conclude that the embedded SFFT is insufficient to model fiber behavior in real composites.

In this paper the SFFT technique is extended to 2-D multiple-fiber arrays (multi-fiber fragmentation test, MFFT) prepared using the rotation device concept developed by Wagner and Steenbakkers [30] with modifications made to achieve uniform inter-fiber distances of about 1 μm [31]. The samples were tested and the data archived using the automated tensile tester described in reference [32]. In addition, the epoxy resin formulation is covalently bonded to the glass fiber through a standard silane coupling agent and formulated to limit the damage associated with fiber fracture to fiber-matrix debonding only. The motivations for this approach are three-fold: (a) To eliminate premature specimen failure that arises from the coalescence of matrix cracks [33], (b) To simplify the complex fiber-fiber interactions around a fiber break (Figure 2) and establish a framework for addressing these more complicated failure modes in a systematic manner, and (c) To fundamentally probe matrix crack suppression and its impact on composite toughness [34]. The objective of this paper, however, is to determine whether the spatial distribution of fiber break centroids for such fibers is best modeled by a uniform distribution on a per-fiber basis (a result previously obtained for single, isolated, non-interacting fibers in 2009 [9]). This is done to facilitate study of the effects that fiber-fiber interactions have on the matrix-fiber stress transfer process.

METHODS[1]

E-glass fibers treated with 3-aminopropyl triethoxy-silane (A-1100) were used. The epoxy matrix consists of the diglycidyl ether of bisphenol-A (DGEBA, Epon 828, Shell Co.), 1,4 butanediol diglycidyl

[1] Certain commercial equipment, instruments, materials, services, or companies are identified in this paper in order to specify adequately the experimental procedure. This in no way implies endorsement or recommendation by NIST.

ether (DGEBD, RD-2, Ciba-Geigy), and meta-phenylene diamine, (m-PDA, Fluka Chemical Co.) that are mixed at a mass fraction ratio of 100:25.1:20.6.

Multi-fiber fragmentation specimens (dogbones) were made using the device described in reference [31] and the procedure for preparing dogbone fiber specimens described by Drzal [35]. The resin mixture was cured for 3 h at 60 °C and 2 h at 121 °C. This cure profile yields an epoxy matrix with the following properties: (a) T_g of = 108 °C, (b) strain-to-failure of ≈ 10 %, and (c) yield strength of ≈ 80 MPa. For comparison the commonly used DGEBA/m-PDA matrix has a T_g of ≈ 126 °C, strain-to-failure of ≈ 6 %, and yield strength of ≈ 70 MPa.

These specimens were then mounted in the custom-built automated fragmentation tester [32]. The fragmentation specimen was deformed by sequential increments (strain steps) with a loading rate of 0.85 mm/min for 35 steps with a 10 min interval between each loading step. Overlapping pictures of the strained fiber(s) were obtained using an Ealing 25X 25-0514 reflecting objective attached to an Electrim 1000L camera that scans the specimen gauge length [32]. The overlapping pictures are stitched together to produce a Time Delay and Integration (TDI) image that is 20 MB in size.

Break locations in each TDI image are digitized manually using the *Digimizer* software package. To minimize gripping effects, only the breaks in the central two-thirds of the gauge length (≈ 16 mm, calibrated region [36]) are selected for analysis [9]. Sections of the TDI image showing the left (annotated by start) and right (annotated by end) dashed lines of the calibrated region for the bundle fibers are shown in Figure 3 for the specimen after it has been returned to zero load. In Table 1, the total number of visible breaks and the number of breaks in the calibrated region [9] are given, along with two estimates of the calibrated region length for a typical single fiber specimen (single fiber 1) and each fiber in a representative bundle specimen (e.g., Bundle Fiber 1, 10 min). The first measure is the distance between the centroid locations of the first and last breaks in the calibrated region. The second measure averages the distance between the location of each end break (first and last breaks) in the calibrated region with the next break outside of this region to arrive at an effective length.

These break coordinate data were then fitted to a number of statistical distributions to determine their goodness-of-fit. The expected locations of the fiber break centroids may be calculated using appropriate formulas for the Uniform, Weibull, and other distributions [3,4,9,37,38]. Consistent with previous findings for the SFFT [9], the Uniform distribution data are presented in this paper since these fits are superior to those based on the Weibull and other distributions.

Uniform probability plots, which plot percentiles of the data against percentiles of the standard uniform distribution, were used to fit the actual break locations. In the version of the plot used here, the ordered break locations are plotted against standard uniform order statistic medians [39] which are defined as [40]:

Equation 2

$$m_1 = 1 - m_n \;;\; m_i = (i - 0.3175)/(n + 0.365),\ i = 2,3,\ldots,(n-1);\ m_n = 0.5^{1/n},\ i = n$$

The correlation coefficient (the probability plot correlation coefficient or PPCC) of the points on this plot provide a direct assessment of goodness of fit.

RESULTS AND DISCUSSION

Comparison of Fiber Break Evolution in Single and Bundle Fiber Samples

A first indicator of behavior from the embedded fragmentation tests are the spatial distribution of breaks along each of the single- and bundle-fibers. The evolution of the break distribution along a fiber in the SFFT is shown in Figure 4(top plots). Here, the break locations (y-axis) are plotted against the percentiles of a uniform distribution rescaled to units of the data (x-axis). It can be seen that beyond a certain stage in the testing there is a tight adherence of all points to the 45° test line, indicating almost perfect agreement with the uniform, with increasing strain (time). A typical graph for the individual fibers of a 2-D 6-fiber bundle (MFFT) is shown in Figure 4(bottom plots). Once more, it can be seen that for each of these fibers, there is a tighter adherence of all points to the 45° test line as strain increases, with progres-

sively increasing value for the PPCC, demonstrating a high degree of uniformity in break locations for each of the bundle-fibers.

A second indicator of fragmentation behavior is the number of breaks at saturation observed along the gauge length of single fiber versus multiple fiber samples. For the system being investigated, a single fiber test sample generally yields about 50 breaks at saturation (Figure 5a), which is contrast with ≈ 40 breaks for close spaced bundle fibers (Figure 5b). It is clear by inspection of the break count data that in all cases saturation (cessation of fiber breaks) has been reached.

In Figure 5a, the number of breaks at saturation in the single fiber specimens ranges from 47 to 54. In the six-fiber bundle sample (Figure 5b), fibers 2 to 6 display between 38 and 40 breaks, while fiber 1 has 48 breaks. For the 6-fiber bundle specimens that have been tested, the number of breaks in the edge of bundle fibers can typically exceed the core fibers by up to 4 breaks, with this increase possibly being associated with the presence of only one constraining fiber.

Examples of statistically co-located fiber breaks are shown in Figure 6 for two sections of the Sample 1-1 6-fiber array. At the strain level of 4.4 % strain there are slight distortions in the matrix around each set of co-located breaks and in addition to the debonding that occurs during fiber fracture there are indications of additional partial debonding along the edge of some fibers which suggest to the authors that this partial debonding is localized in the plane of the 2-D fiber array and may occur because of the complicated shear stress field that exists between the co-located fiber breaks. The inter-fiber distance (∅) at this strain level ranges from 1.3 to 2. Section 1 of the 6 fiber array is shown again in Figure 7 at 8.4 % strain. The matrix distortions around the co-located breaks that existed at 4.4 % strain are prominent and the partial debonding on the edge of the fibers in the fiber break regions appears to have grown. The new set of co-located fiber breaks also exhibits evidence of partial debonding and some matrix distortion. As expected, ∅ is on average smaller and ranges from 0.7 to 1.7 at 8.4 % strain.

Interpretation of the Fiber Break Location Data

The Fiber Break Evolution Process in a 2-D Epoxy/Glass Multi-Fiber Array

The break data indicate that the fragmentation processes of single- and bundle-fibers are essentially statistically equivalent, regardless of any stress transfer activity between adjacent, proximate fibers such as, stress concentration effects that induce statistically co-located fiber breaks in adjacent fibers of the array (i.e, a fiber-fiber interaction effect). In Figure 4(top), the break location data evolves into a statistical uniform spacing after 31 breaks with a PPCC of 0.9984 and remains uniform with a slight PPCC increase to 0.9995 during the occurrence of the additional 19 breaks. At 29 breaks in the array fiber shown in Figure 4(bottom), the PPCC for the uniform distribution is 0.9992 and remains essentially unchanged during the 15 additional breaks that precede the onset of saturation. This is particularly interesting since the number of fiber breaks in the array whose inter-fiber spacing is nominally 1 μm have ≈ 20 % less breaks than those observed in a SFFT specimen. This decrease formed the basis of concern by Li et al. [29] about the applicability of SFFT results in composite failure models.

The single fiber data agrees with an earlier publication [9] where break location data on un-sized E-glass/DGEBA/m-PDA SFFT specimens were studied. In that research, the fiber length data from one SFFT specimen was tabulated. These length data showed that the uniform distribution of breaks was achieved at the point where ≈ 60 % of the fragment length was excluded from additional fracture because of the presence of exclusion zones arising from the break process. Beyond this point 39 % of the remaining fiber breaks that occurred generated fragments of approximately equal spacing, where equality was defined as two daughter fragments whose lengths differ by less than 40 μm. In spite this high occurrence of equal break events the break locations remained uniform.

Excluding the first bundle fiber data, there is a difference of approximately 8 to 10 breaks between the single- and bundle-fibers, which is consistent with the data of Li et al. [29]. Others [41,42] who have observed this change have interpreted the difference in breaks between SFFT and MFFT type specimens through the lens of the K-T model. This practical engineering estimate of IFSS assumes the matrix is elastic-perfectly plastic and has no adjustable parameters to account for changes in break density due to stress concentration effects and other fiber-fiber interactions that may occur in composite specimen. Based on this model, the decrease in the number of breaks reflects a change in IFSS between the SFFT

and MFFT specimen, thereby suggesting that the IFSS is not a materials property. This outcome becomes problematic for those seeking to develop unidirectional composite failure models based on micromechanics output data [43,44].

It must be noted at this point that the research of Ohsawa et al. [45] shows the critical fragment length in glass fiber reinforced thermosetting resins to be temperature dependent, thereby indicating that the resin is a nonlinear thermoviscoelastic material. In contrast to the interpretation afforded by the K-T model, Li et al. [29] interpreted the change as arising from the presence of neighboring fibers preventing the failure at some flaws without discussing explicitly how this might occur. This interpretation considers the IFSS to be a material property, albeit dependent on temperature and rate, with a fiber-fiber interaction effect superimposed on the normal SFFT stress transfer process in a way that effectively increases the observed critical transfer length in array fibers.

Some Thoughts on the Increase in the Critical Transfer Length

Li et al. in referencing the original research by Cox [6] noted that this shear-lag model includes a fiber volume fraction effect, which they denoted as r_e. For composite analyses [46], this parameter replaces r_m in Equation 1b and takes a value equal to the center-to-center inter-fiber distance. Hence, as the inter-fiber distance gets smaller, the critical transfer length is supposed to get smaller. Since there is no adjacent fiber in a SFFT specimen, r_m carries the definition of a distance perpendicular from the fiber which beyond this point, any deformation in the matrix is assumed to occur as if the fiber and associated fiber breaks are not present [47,48]. This intractable parameter has been estimated to be 10 to 15 fiber radii [47], with the research of Li et al. suggesting an effective value for significant interaction with the adjacent fiber being no more than 12 fiber radii.

One way to visualize and approximate r_m is to examine the birefringence in the matrix around a fiber break. In Figure 2, several array fibers are shown with associated birefringence patterns that demarcate the area of perturbed matrix material around an associated fiber break. The bottom fiber in Figure 2a is far enough away from the other fibers that its birefringence patterns do not interact with the adjacent

fibers. The perpendicular distance of the perturbed matrix away from this fiber has been estimated to be $\approx 5r_f$ and this value may be taken in this example as a maximum effective distance for r_m. For the closer spaced fibers these perturbed areas interact with similar areas in adjacent fibers in a complicated manner that appears to be also tied to the small but perceptible matrix cracks associated with each fiber break. Furthermore, the size of r_e does not lend itself to the simple estimate used by Cox. Figure 2b shows the perturbed matrix material interacting with the adjacent fiber and appearing to go beyond the fiber. Although we cannot be sure at this point this may be due to the unconstrained but perturbed matrix material above and below the 2-D fiber plane.

The non-equivalence of r_e and r_m is shown schematically in Figure 8(a,b). Consistent with the research of Galiotis, the radius of matrix (r_m) parameter as defined in the Cox model (Equation 1b) is drawn with a value of $10r_f$, while r_e depends on the interfiber spacing and has a value in Figure 8b of $6r_f$. Data from Li et al. [29] indicates a value for r_m of $\approx 12r_f$.

The Radius of Matrix (r_m) Parameter and Bundle Fiber 1

In 1965, Tyson and Davies [49] estimated that the IFSS ($\tau_i\{z\}$) causes shear stresses in the matrix ($\tau_m\{z,r\}$) near a fiber break. These stresses were assumed to decrease radially as the inverse of the distance from the fiber axis.

Equation 3

$$\frac{\tau_m\{z,r\}}{\tau_i\{z\}} = \frac{1}{r}$$

A more complicated expression was deduced in 1969 by Amirbayat and Hearle [48] (Equation 4) using the matrix free body diagram of Figure 1 that depends on the radius of matrix (r_m) parameter.

Equation 4

$$\frac{\tau_m\{z,r,r_f,r_m\}}{\tau_i\{z\}} = \frac{r_f}{r}\left[1 - \frac{\left(\frac{r^2}{r_f^2} - 1\right)}{a}\right]$$

$$a = \frac{A_m}{A_f} = \frac{\pi r_m^2 - \pi r_f^2}{\pi r_f^2}$$

where

$\tau_m\{z,r,r_f,r_m\}$	denotes the interfacial shear stress in the matrix at a distance r from the fiber axis. Note that this parameter is dependent on r_m through the term a.
$\tau_i\{z\}$	denotes the interfacial shear stress along the fiber axis (z-direction) as derived in Cox-type shear-lag models.
r_f	denotes the radius of the fiber
A_m, A_f	denotes the cross-sectional area of the matrix surrounding the fiber and fiber, respectively
r_m	denotes the radius of the matrix surrounding the fiber beyond which the matrix deformation is not influenced by the presence of the fiber [47].

It can be theorized from Galiotis' definition that for a given molecular level of fiber-matrix adhesion there is a volume of matrix that is needed to completely transfer the stress between the matrix and embedded fiber around a fiber break. In the Cox-type shear-lag models, this volume is represented as a cone with the maximum IFSS occurring at the fiber fragment ends that are formed when the fiber fractures (Figure 1). The intensity of the shearing forces in this cone of matrix material ($\tau_m\{z,r,r_f,r_m\}$) is dependent on $\tau_i\{z\}$.

From the above discussion, one can infer that when fibers are placed within the cone of sheared matrix as defined by the Amirbayat and Hearle (A-H) Cox model [48] (Figure 1), the shearing forces in the matrix that are associated with a fiber break interact at the adjacent fiber interface increasing the localized strain in that fiber, which increases the local stress in the fiber and results in an increased probability of a transversely aligned break [50]. In Figure 9, estimates of the normalized maximum shear stress that an adjacent fiber might experience from a broken fiber are plotted as a function of inter-fiber separation (in diameter units) using the A-H equation and the $1/r$ estimate made by Tyson and Davies.

Finally, the key question in relating r_m to r_e is: How does the efficiency of the stress transfer process change when adjacent fibers, such as those found in a real composite, are placed within this cone of sheared matrix material? The equivalence of the uniform break distributions in the single- and multi-fiber microcomposites together with the reduction in the break density for closely spaced array fibers suggests to the authors that the transfer efficiency may be reduced in the MFFT case. The exact nature of the fiber-fiber interactions that may cause a reduction in transfer efficiency and possibly increase the critical transfer length must be investigated.

The role of the matrix distortion that is observed in the region around the co-located fiber breaks on the critical transfer length must also be reconciled, since this distortion may reflect localized yielding. This phenomenon is not observed in the SFFT specimens (Figure 7) and may be a direct result of the complicated shear field that exist between fibers with co-located fiber breaks since the intensity of this distortion appears to increase with increasing strain (compare section 1 in Figure 6 and Figure 7). Additionally, many of the array fiber breaks (e.g., Figure 7 section 1) also show evidence of partial debonding. This debonding occurs along the edge of the fibers in the region where matrix distortion is prevalent. Without additional research, one can only speculate about the extent to which matrix yielding and partial debonding contribute to a reduction in stress transfer efficiency in the multi-fiber arrays.

CONCLUSIONS

A multi-fiber fragmentation test has been applied to parallel arrays of E-glass fibers embedded in a DGEBA matrix under uni-axial tension. The adherence of the break location distribution to uniform be-

havior is validated using probability plotting and associated correlations that are higher (> 0.99) than those obtained when using either two- or three-parameter Weibull models to describe the same distribution (see supplemental material). The PPCC of the uniform probability plots was consistently, significantly high beyond a certain number of strain steps. The values ranging from 0.9993 to 0.9996 confirm an underlying uniform spatial distribution of fiber breaks in each fiber of a MFFT specimen that is consistent with results obtained previously on SFFT specimens [9]. These results suggest that the cumulative distribution function (CDF) for the fragment lengths of any fiber at saturation in MFFT specimens should conform to the expression deduced by Whitworth and referred to by others [2-4].

Secondly, single fibers are mostly characterized by shorter average fragment lengths when compared to bundle-fibers, a comparison similar to that published by Li et al. (1995). This result is a direct contradiction of the prediction made by the family of shear-lag theories, which predict that bundled fibers should have shorter average fragment lengths. From these results it can be theorized that efficiency of stress transfer along a fiber in a closely spaced array is less than that observed in a comparable single fiber. This inefficiency results in an effective increase in the critical transfer length.

Overall, these results demonstrate the necessity in the absence of an accurate model for direct measurement for fiber fragmentation of bundled fibers, since fragment length results for single fibers are not necessarily representative of those for bundled fibers. The need to be able to prepare, test and analyze large numbers of specimens is highlighted, so that statistically significant and scientifically valid results can be obtained. This objective is greatly aided by custom-built equipment for coupon preparation, specimen testing, and data analysis at NIST. Improvements in such automated processes are expected to expedite fragmentation tests, remove manual manipulation as a contributing factor, and further the objective of developing a standard protocol for the measurement of interfacial shear strength.

Acknowledgements

The authors would like to thank the following people for their helpful discussions of this paper:

Drs. Christopher Hartshorn, Young Lee, Jonathan E. Seppala.

REFERENCES AND NOTES

1. L. S. Norwood, in "Handbook of Polymer Composites for Engineers", L. Hollaway, Ed., Woodhead Publishing Limited: Cambridge, UK (1994) p 9.
2. W. A. Whitworth, "Choice and Change: An Elementary Treatise on Permutations, Combinations, and Probability", Cambridge University Press: London, (1887)
3. Read, C. B., "Spacings", In: Encyclopedia of Statistical Sciences, Kotz, S. and Johnson, N. L. (eds); John Wiley & Sons: New York, 8 (1988) 566-569.
4. R. Pyke, *J Roy Stat Soc B Met*, 27, 395 (1965)
5. L. Holst, *J Appl Probab*, 17, 623 (1980)
6. H. L. Cox, *Brit J Appl Phys*, 3, 72 (1952)
7. A. Kelly; W. R. Tyson, *J Mech Phys Solids*, 13, 329 (1965)
8. R. B. Henstenburg; S. L. Phoenix, *Polym Compos*, 10, 389 (1989)
9. J. H. Kim; S. D. Leigh; G. Holmes, *Journal of Polymer Science Part B*, 47, 2301 (2009)
10. G. A. Holmes; R. C. Peterson; D. L. Hunston; W. G. McDonough, *Polym Compos*, 28, 561 (2007)
11. L. T. Drzal; M. J. Rich; J. D. Camping; W. J. Park, "Proceedings of the 35th Annual Technical Conference", Reinforced Plastics/Composites Institute and The Society of the Plastics Industry, Inc., p 1.
12. J. A. Nairn, *Mech Mater*, 13, 131 (1992)
13. D. Tripathi; F. R. Jones, *J Mater Sci*, 33, 1 (1998)
14. J. M. Whitney; L. T. Drzal, in "Toughened Composites", N. J. Johnson, Ed., ASTM: Philadelphia, PA (1987) p 179.
15. D.-A. Mendels, Analysis of the Single-Fibre Fragmentation Test; NPL Reprot MATC(A)17; National Physical Laboratory, Teddington, Middlesex, 2001.
16. M.J. Lodeiro, Single-Fibre Fragmentation Test for the Characterisation of Interfacial Phenomena in PMCs; NPL Report MATC(MN)07; National Physical Laboratory, Teddington, Middlesex, 2001.
17. M.J. Lodeiro, Investigation of PMC Interface Properties Using the Single-Fibre Fragmentation Technique; NPL Report MATC(A)16; National Physical Laboratory, Teddington, Middlesex, May 2001.
18. Y. Dai; X. Ji; L. Ye; Y. W. Mai, *Compos Interface*, 13, 67 (2006)
19. D. Tripathi; F. Chen; F. R. Jones, *P Roy Soc A-Math Phy*, 452, 621 (1996)
20. T. J. Copponnex, *Compos Sci Technol*, 56, 893 (1996)
21. P. Feillard; G. Desarmot; J. P. Farve, *Compos Sci Technol*, 50, 265 (1994)
22. P. Feillard; D. Rouby; G. Desarmot; J. P. Favre, *Mat Sci Eng A-Struct*, 188, 159 (1994)
23. K. Goda; J. M. Park; A. Netravali, *J Mater Sci*, 30, 2722 (2013)
24. C. Y. Hui; S. L. Phoenix; D. Shia, *Compos Sci Technol*, 57, 1707 (1997)
25. C.-Y. Hui; S. L. Phoenix; D. Shia, *Compos Sci Technol*, 57, 1707 (1997)
26. W. A. Curtin, *J Mater Sci*, 26, 5239 (1991)
27. W. D. Bascom; R. M. Jensen, *J Adhesion*, 19, 219 (1986)
28. A. N. Netravali; R. B. Hestenburg; S. L. Phoenix; P. Schwartz, *Polym Compos*, 10, 226 (1989)
29. Z. F. Li; D. T. Grubb; S. L. Phoenix, *Compos Sci Technol*, 54, 251 (1995)
30. H. D. Wagner; L. W. Steenbakkers, *J Mater Sci*, 24, 3956 (1989)
31. J.-H. Kim; J. W. Hettenhouser; C. K. Moon; G. A. Holmes, *J Mater Sci*, *44*, 3626 (2009)

32. G. Holmes; S. Wesson; W. G. McDonough; J. H. Kim; A. Netravali; J. N. Walker; R. A. Johnson, *J Mater Sci*, *44*, 2007 (2009)
33. G. A. Holmes; W. G. McDonough, "Proceedings of the 47th International SAMPE Symposium and Exhibition", B.M.Rasmussen, L.A.Pilato and H.S.Kliger,Eds., Society for the Advancement of Material and Process Engineers (SAMPE), Covina, CA, (May 2002), p 1690.
34. E. K. Drown; H. Almoussawi; L. T. Drzal, *Journal of Adhesion Science and Technology*, 5, 865 (1991)
35. L. T. Drzal; P. J. Herrera-Franco, in "Engineered Materials Handbook: Adhesives and Sealants", C. A. Dostal, M. S. Woods, A. W. Ronke, S. D. Henry, and J. L. Daquila, Eds., ASM Int.: Metals Park, Ohio (1990) p 391.
36. The start and end of the calibrated region corresponds to a distance sufficiently removed from the load application (grips) that stress pertubations that may influence the fiber break pattern are minimized in accords with Saint-Venant's principle.
37. C. Forbes; M. Evans; N. Hastings; B. Peacock, "Statistical Distributions", Wiley: (2011)
38. H. Rinne, "The Weibull Distribution: A Handbook", CRC Press: Boca Raton, (2009)
39. The order statistics of an N-fold sample are the sorted data points. The minimum value is the 1st order statistic and the maximum value is the Nth order statistic. Order statistics drawn from an N-fold sample generated from a prescribed distribution, such as the uniform, exhibit predictable, calculable behavior. So, for example, the distribution of the Kth order statistic drawn from an N-fold uniform sample can be computed, as can its mean, variance, median, mode etc.
40. J. J. Filliben, *Technometrics*, 17, 111 (1975)
41. S. Luan; H. Li; Y. Jia; L. An; Y. Han; Q. Xiang; J. Zhao; J. Li; C. C. Han, *Polymer*, 47, 6218 (2006)
42. J. M. Park; S. I. Lee; J. W. Kim; D. S. Kim, *Polym-Korea*, 22, 659 (1998)
43. S. Blassiau; A. R. Bunsell; A. Thionnet, *Proceedings of the Royal Society A-Mathematical Physical and Engineering Sciences*, 463, 1135 (2007)
44. S. Blassiau; A. Thionnet; A. R. Bunsell, *Compos Sci Technol*, 69, 33 (2009)
45. T. Ohsawa; A. Nakayama; M. Miwa; A. Hasegawa, *Journal of Applied Polymer Science*, 22, 3203 (1978)
46. J. A. Nairn, *Mech Mater*, 26, 63 (1997)
47. C. Galiotis, *Compos Sci Technol*, 42, 125 (1991)
48. J. Amirbayat; J. W. S. Hearle, *Fibre Sci Technol*, 2, 123 (1969)
49. W. R. Tyson; G. J. Davies, *British Journal of Applied Physics*, 16, 199 (1965)
50. D. T. Grubb; Z. F. Li; S. L. Phoenix, *Compos Sci Technol*, 54, 237 (1995)

The Fiber Break Evolution Process in a 2-D Epoxy/Glass Multi-Fiber Array

Table 1. Total number of visible breaks and breaks in the calibrated region along with two estimates of the calibrated region length for a typical single fiber and fibers from a 2-D multi-fiber array.

	Fiber Break Count		Calibrated Region Length, μm	
Specimen	Total	Calibrated Region	First to Last Break (Centroid to Centroid)	Effective Length (Averaged)
Single Fiber 1	62	47	16,225	16, 585
Bundle Fiber 1	57	48	16,342	16,718
Bundle Fiber 2	48	40	16,337	16,703
Bundle Fiber 3	48	39	16,332	16,705
Bundle Fiber 4	47	38	16,422	16,749
Bundle Fiber 5	48	39	16,330	16,692
Bundle Fiber 6	49	40	16,370	16,715

FIGURES

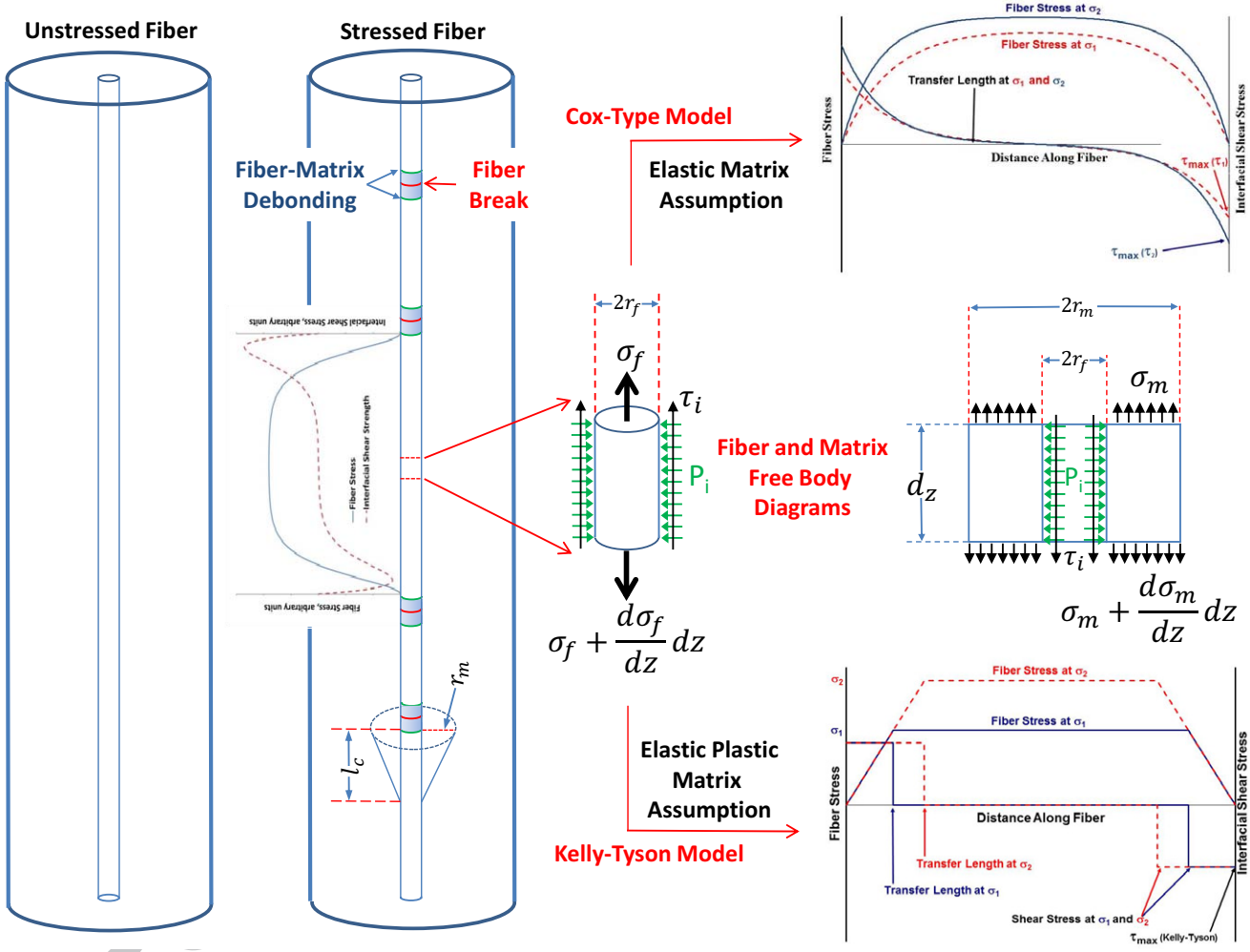

Figure 1. Principle of the fragmentation test. Free body diagrams for developing models of the fiber-matrix interface stress-transfer process and the magnitude of the shearing forces that emanate radially into the matrix. (*adapted from [48]*)

The Fiber Break Evolution Process in a 2-D Epoxy/Glass Multi-Fiber Array

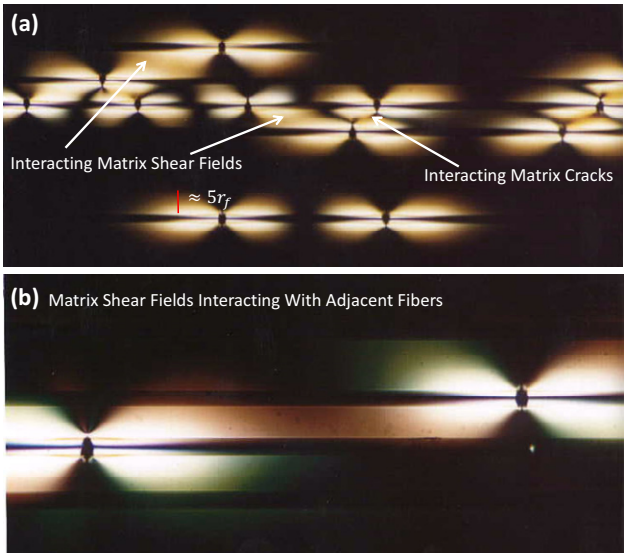

Figure 2. Elliptical birefringence patterns of highly stressed epoxy near the E-glass fiber fragment ends in 2-D multi-fiber E-glass/DGEBA/m-PDA microcomposites. The thickness and length of the stressed regions give some indications of the size of $\boldsymbol{r_m}$ and $\boldsymbol{l_c}$. The interaction between shear fields and matrix cracks can be observed in (a) and the interaction between the stressed matrix region and adjacent fibers can be observed in (b).

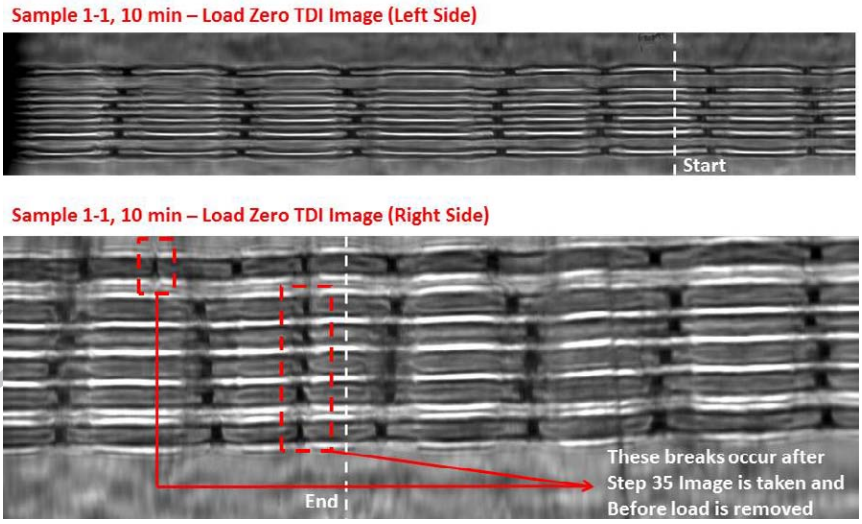

Figure 3. Partial TDI image of bundle fibers showing the left and right ends of the calibrated region. The enclosed breaks in fibers 2 through 6 document the occurrence of time-dependent coordinated fiber failure in a multi-fiber array. These breaks were not in the TDI image (not shown) taken 10 min after the final step strain (No. 35).

The Fiber Break Evolution Process in a 2-D Epoxy/Glass Multi-Fiber Array

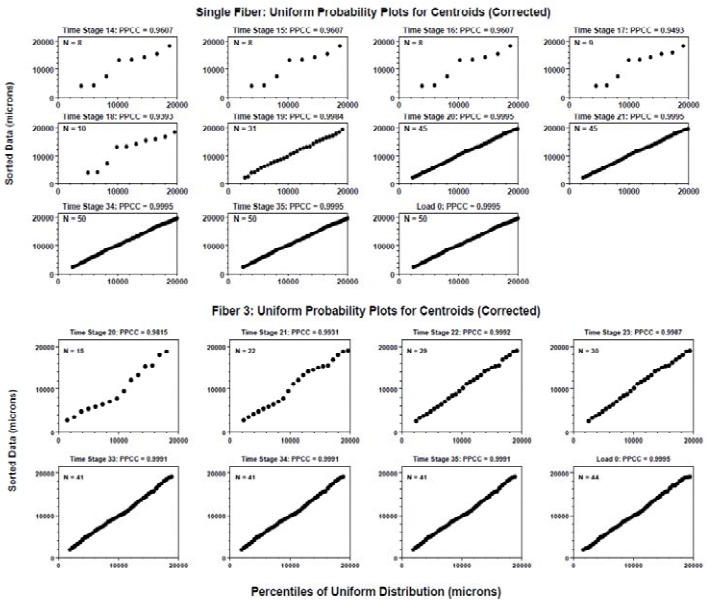

Figure 4. Uniform Plot for break locations of a single fiber (top) and an array fiber (Fiber 3, bottom) every ten min for 360 min. Actual break co-ordinates (Y-axis) are plotted against co-ordinates calculated for a Uniform break centroid distribution (X-axis). Final plot (Load 0 for each specimen) plots co-ordinates for Stage 35 when specimen has been relaxed from its final deformation.

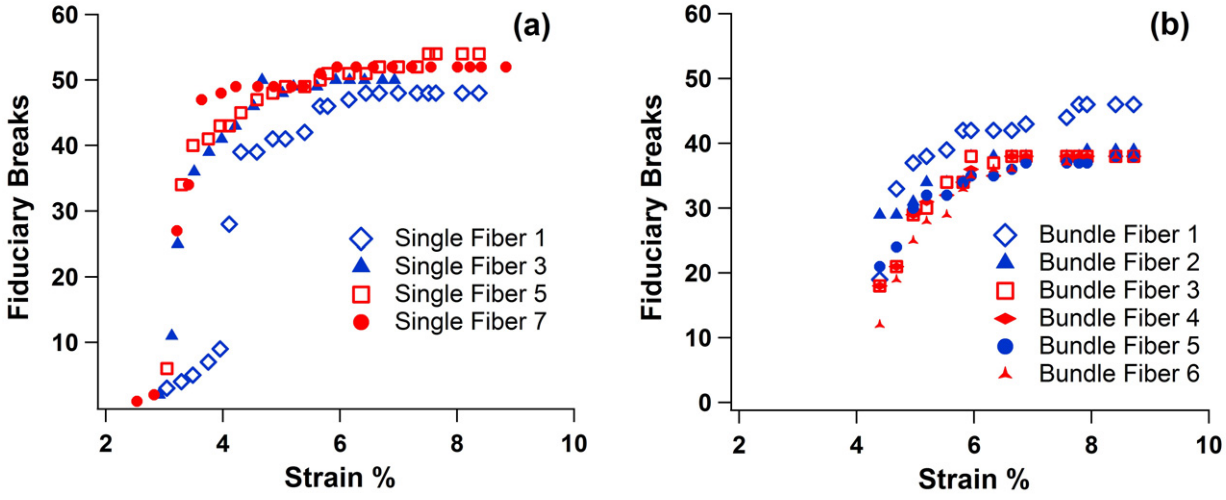

Figure 5. Number of gauge length breaks for four single fibers (Figure 5a), compared with that of six individual fibers from a six-fiber bundle (Sample 1-1) (Figure 5b)

The Fiber Break Evolution Process in a 2-D Epoxy/Glass Multi-Fiber Array

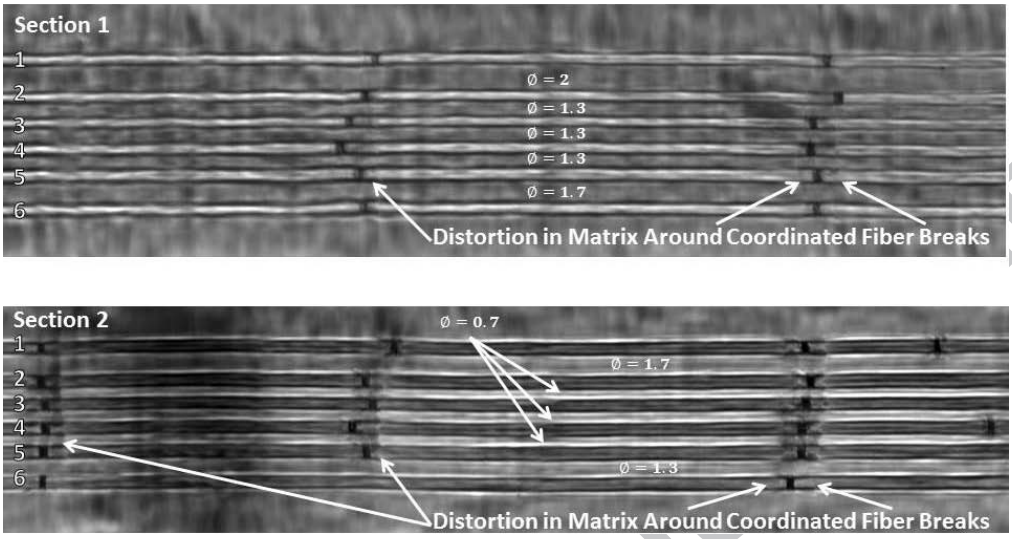

Figure 6. Two sections from the Sample 1-1 6-fiber array at approximately 4.4 % strain. Ø denotes the distance in fiber diameters between adjacent fibers.

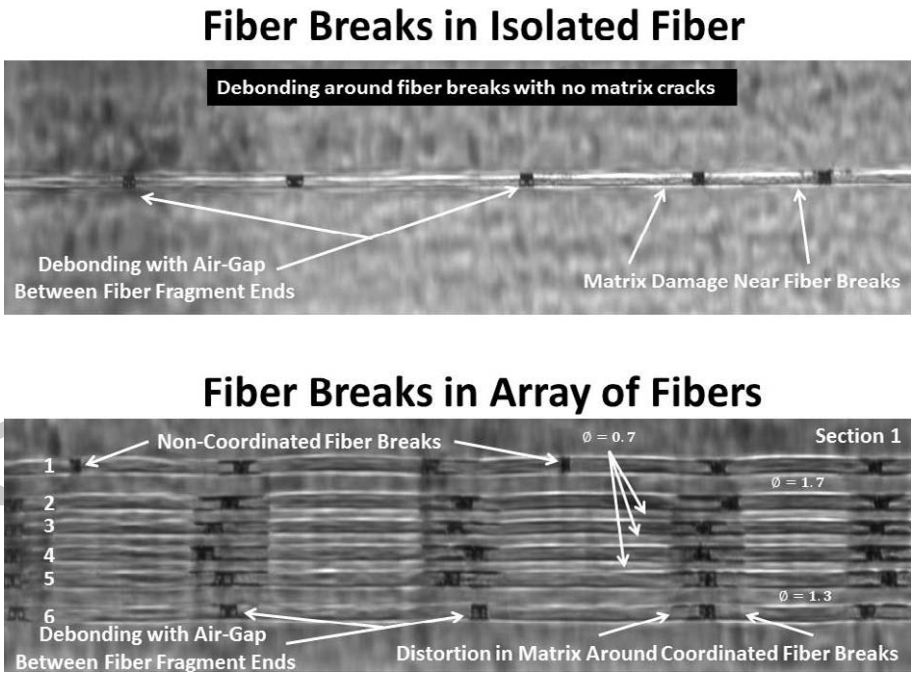

Figure 7. Fiber breaks in a single fiber composite and section 1 of Sample 1-1 6-fiber array at approximately 8.4 % strain. Observe the debonding and air-gaps between fiber fragment ends that become increasingly visible with increasing strain in both samples and the matrix distortion in the immediate vicinity of coordinated fiber breaks. Ø denotes the distance in fiber diameters between adjacent fibers.

The Fiber Break Evolution Process in a 2-D Epoxy/Glass Multi-Fiber Array

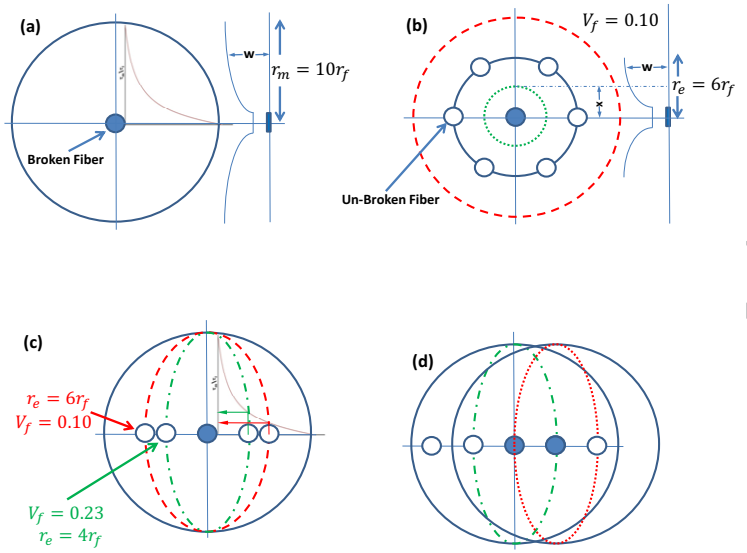

Figure 8. Schematic representations of radius of matrix parameters at fiber break end as defined by Cox model: (a) $\boldsymbol{r_m = 10r_f}$ in single fiber composite with decrease in relative intensity superimposed, (b) $\boldsymbol{r_e = 6r_f}$ in composite with break surrounded by hexagonal array of fibers ($\boldsymbol{V_f = 0.10}$), (c) potential distortion in 2-D multi-fiber array with fiber spacing $\boldsymbol{r_e = 4r_f}$ & $6\boldsymbol{r_f}$ in fiber plane, (d) unknown distortion in 2-D multi-fiber array with two aligned broken fibers with fiber spacing $\boldsymbol{r_e = 4r_f}$ in fiber plane.

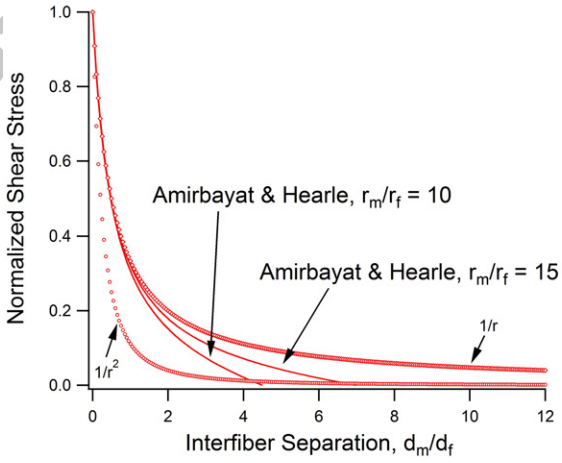

Figure 9. Estimate of the matrix shearing forces that an adjacent fiber might experience as a function of interfiber separation.

The Fiber Break Evolution Process in a 2-D Epoxy/Glass Multi-Fiber Array